PCCP

PAPER

View Article Online
View Journal | View Issue

Cite this: *Phys. Chem. Chem. Phys.*, 2018, **20**, 17289

Oxyhydroxide of metallic nanowires in a molecular H_2O and H_2O_2 environment and their effects on mechanical properties

Gurcan Aral, *[a] Md Mahbubul Islam, [b] Yun-Jiang Wang, [c] Shigenobu Ogata [de] and Adri C. T. van Duin[f]

To avoid unexpected environmental mechanical failure, there is a strong need to fully understand the details of the oxidation process and intrinsic mechanical properties of reactive metallic iron (Fe) nanowires (NWs) under various aqueous reactive environmental conditions. Herein, we employed ReaxFF reactive molecular dynamics (MD) simulations to elucidate the oxidation of Fe NWs exposed to molecular water (H_2O) and hydrogen peroxide (H_2O_2) environment, and the influence of the oxide shell layer on the tensile mechanical deformation properties of Fe NWs. Our structural analysis shows that oxidation of Fe NWs occurs with the formation of different iron oxide and hydroxide phases in the aqueous molecular H_2O and H_2O_2 oxidizing environments. We observe that the resulting microstructure due to pre-oxide shell layer formation reduces the mechanical stress *via* increasing the initial defect sites in the vicinity of the oxide region to facilitate the onset of plastic deformation during tensile loading. Specifically, the oxide layer of Fe NWs formed in the H_2O_2 environment has a relatively significant effect on the deterioration of the mechanical properties of Fe NWs. The weakening of the yield stress and Young modulus of H_2O_2 oxidized Fe NWs indicates the important role of local oxide microstructures on mechanical deformation properties of individual Fe NWs. Notably, deformation twinning is found as the primary mechanical plastic deformation mechanism of all Fe NWs, but it is initially observed at low strain and stress level for the oxidized Fe NWs.

Received 16th April 2018,
Accepted 4th June 2018

DOI: 10.1039/c8cp02422g

rsc.li/pccp

1. Introduction

Unfortunately, readily formation of thin oxide layers on the exposed surface of Fe materials is naturally inevitable during their production, storage, and working conditions.[1–4] There is no effective way of preventing progressive oxidation of reactive metallic materials, specifically when they are exposed to reactive ambient conditions.[2–4] The surface oxidation can be circumvented only under extremely high vacuum conditions or with specific surface coatings.[1,4,5,7–9] Generally, in aqueous working conditions, metallic Fe materials commonly produce various crystalline phases of Fe oxide and oxyhydroxide such as green rust ($Fe(OH)_2$), goethite (α-FeOOH), *etc.*[3,6,10–13]

Overall, progressive oxidation of metallic Fe materials is usually associated with corrosion, and the corresponding detrimental effects are prevalent in many practical applications of the materials.[1–3,6,10] The environmental conditions dictate the strength, lifetime, and failure of reactive metallic materials.[3,14,15] In particular, the resulting oxide shell layer drastically alters the physical and chemical properties of the exposed surface layer, and as a result, eventually, the strength of Fe NWs may be weakened substantially compared to the corresponding un-oxidized counterparts.[2,3,10,16,17] However, the presence of undesirable oxide shell layer (or desirable oxide-coating) on the free Fe NW surfaces is associated with surface/interface finite-size effects which help distinctly to achieve potentially additional interesting and unique chemical,[3] physical,[8] optical,[18] mechanical,[17] and magnetic properties[5,8,11] as compared to the un-oxidized counterparts.[4,10,12,19–21] All of these unique features make oxide-coated Fe-based nanomaterials very promising in many different research areas.[1,4,5,7–9] The Fe nanomaterials and their oxide-coated derivatives have been successfully used in many

[a] *Department of Physics, Izmir Institute of Technology, Urla, Izmir, 35430, Turkey. E-mail: gurcanaral@iyte.edu.tr; Fax: +90 (232) 750-7707; Tel: +90 (232) 750-7717*
[b] *School of Materials Engineering, Purdue University, West Lafayette, Indiana 47907, USA*
[c] *State Key Laboratory of Nonlinear Mechanics, Institute of Mechanics, Chinese Academy of Sciences, Beijing 100190, China*
[d] *Department of Mechanical Science and Bioengineering, Osaka University, Osaka 560-8531, Japan*
[e] *Center for Elements Strategy Initiative for Structural Materials (ESISM), Kyoto University, Kyoto 606-8501, Japan*
[f] *Department of Mechanical and Nuclear Engineering, The Pennsylvania State University, University Park, PA 16802, USA*

nanoscale applications such as in biomedical science,[5,7,13] magnetic data storage, *etc.*[4,5,20] Nowadays, of special interest, oxide-coated Fe NWs are either used as a typical core–oxide shell layer (Fe–Fe_xO_y) or a fully oxidized iron material such as in hematite, magnetite and wüstite structures.[1,5,7,11,13,18–23] The diversity (nature) of surface oxide shell layers serve to tune the material properties, which provides a variety of opportunities and challenges to improve Fe NWs properties for various applications.[1,7,8,13,19,23] In particular, relevant surface modifications including a subtle variation of surface oxide chemistry, unique size, shape, oxide shell layer thickness, oxide layer density, constituents, overall morphology, porosity and crystal phase are strongly coupled with intrinsic functional properties as well as correlation with the performance of core–shell structured Fe NWs.[1,7,8,12,20–25] Generally, the presence of an oxide layer on the metallic materials has a pivotal role on various physical and chemical processes such as adsorption/desorption,[7,11,12] corrosion, catalysis,[4,7,11] corrosion,[2,3] and wetting processes.[4,5,9,12,19,21]

Undoubtedly, detailed fundamental understanding of the oxidation mechanism, microstructures of the resulting oxide layers of nanoscale Fe materials, associated with the type of oxidizer in a variety of reactive atmospheres is essential in coating technology as well to understand corrosion processes of Fe metal and steel.[1–4,7,24–27] Especially, reactive H_2O and H_2O_2 environments may provide effective options to control the surface properties of Fe NWs in order to improve their functionality with regard to corrosion resistance and catalytic performance.[2–4,10,13] The overall oxide growth at Fe associated with H_2O and H_2O_2 is usually incorporated consecutively by adsorption, dissociation, segregation, diffusion, and eventually reconstruction on the free surface of Fe nanomaterials *via* physical and/or chemical reactions.[1–4,10,27] In general, oxidation processes cause the creation of various defects on the developed oxide region and the interface between the metallic core of Fe NWs and the oxide shell layer, which influences the mechanical properties of the NWs.[17] Therefore, it is essential to understand quantitatively how H_2O and H_2O_2 molecular species oxidize the metallic Fe NW free surfaces and how the formation of oxidized shell layers affect the mechanical elastic properties and intrinsic strength.

Recently, Landau *et al.* performed experiments to investigate the effect of helium on the mechanical properties, and deformation mechanism of as-fabricated and helium implanted single crystalline iron nanopillars under both tensile and compression loading.[16] They reported that the tensile deformation for both as-fabricated and helium implanted samples display three distinct regimes: elastic loading, substantial strain hardening, and a "steady state" region. For example, the yield and ultimate strength as well as flow stress significantly increase for helium-implanted samples compared to as-fabricated ones. Furthermore, numerous MD studies have been performed to investigate the strengthening of pure Fe NWs using fixed charge interatomic potentials under tensile and compressive loading.[14,15,28–32] In these studies, Fe NWs were considered simply in vacuum, and thereby, the effects of the surface oxide layer on the mechanical behaviors were ignored. Many of these studies have focused on exploring the influence of geometry, size, loading, grain size, surface geometry, and temperature on the mechanical deformation mechanisms and related properties of metallic Fe NWs. These studies demonstrated that the mechanical deformation mechanisms and associated properties of metallic Fe NWs are strongly contingent on these parameters. For example, using the EAM potential, Sainath *et al.* have studied the size effect on the mechanical deformation mechanism of metallic ⟨100⟩/{100} and ⟨110⟩/{111}-oriented single crystal BCC Fe NWs under tensile and compressive loading.[29,30] They observed the crystal orientation dependent behavior of tensile deformation of single-crystal BCC Fe NW for various initially orientated ⟨100⟩, ⟨112⟩, ⟨102⟩, ⟨110⟩ and ⟨111⟩ Fe NWs.[28]

However, only a few recent studies have been conducted to quantify and confirm the importance of surface oxidation on the mechanical properties of metallic NW by using reactive variable charge potential models. Meanwhile, it has been realized that the deformation and related mechanical properties of oxidized metallic nano-materials drastically differ from their un-oxidized counterparts.[17,32–35] It was shown that the mechanical properties at the nanoscale are directly related to surface oxide shell features, such as oxide thickness, type of oxide microstructure, and morphology.[23] For example, in our previous study, MD simulation with ReaxFF potential was used to study the oxidation of Fe NWs with O_2 and the effect of oxidizing layers on the mechanical deformation mechanism and related properties as a function of oxide shell thickness.[17] We found that the thicknesses of the oxide shell layer on the free surface of Fe NWs play an important role in the tensile mechanical properties. Sen *et al.* studied the oxide shell layer dependent deformation mechanism of metallic aluminum (Al) NWs by using the ReaxFF method.[32,33] They reported that the oxide shell layer on the Al NW free surface helps to change the elastic mechanical response from brittle to ductile transition behavior. Our previous studies indicated that the influence of the surface oxide shell layer on the mechanical properties of Ni NWs is most significant for smaller rather than larger diameters.[34]

The effects of each resulting pre-hydroxylated shell layer—occurring due to the reactions with H_2O and H_2O_2 —on the mechanical tensile deformation response of Fe NWs have not been explored yet. For this reason, we have carried out MD simulations using the ReaxFF potential, which was developed by Aryanpour *et al.*[6]

2. Computational approach and methods

2.1 Reactive force field (ReaxFF) potential

The complexity of oxidation of Fe NWs and its effects on the mechanical behaviour is not easily accessible to quantify independently by using existing experimental methods. Particularly, there are difficulties with the high specific surface areas of reactive Fe NWs, as well as small spatio-temporal scale related to the experimental characterization.[16,26] In this respect, MD simulations with fixed charge potential models are limited in describing complex chemical reactions as well as the interfacial properties

of oxide coated Fe NWs. The fixed charge potential models disregard the surface oxidation effects, leading to incorrect predictions of mechanical properties of oxidized Fe NWs.[15,16,26] For these reasons, recently, several variable charge methods have been developed.[6,36,37]

In order to account for the dynamical description of charges as well as the formation and breaking of chemical bonds in complicated reaction processes, we used the ReaxFF reactive force field method.[6,36,37] ReaxFF is a bond order based variable charges method, which enables us to quantify directly the nature of the formation of an oxide shell layer on the free surface of Fe NWs and predict their effects on the mechanical responses.[17] The ReaxFF Fe/O/H force field, developed by Aryanpour *et al.*, is used in this study to describe accurately the entire range of intermediate interactions among Fe/O/H atoms including both covalent and ionic bonds, and capture the bond formation and breaking.[6] The Fe/O/H force field has already demonstrated its capability in predicting the mechanical properties of Fe NWs as a function of oxide shell layer thicknesses.[17] Using the force field, we performed MD simulations to make quantitative predictions as well as elucidate the influence of the oxidized shell layer on mechanical properties and provide atomistic insight into the mechanical deformation process of [001]-oriented Fe NWs. The details of the ReaxFF method can be found in recent reviews.[6,38,39]

2.2 Set-up of simulation system and computational methods

We performed the MD simulations with the ReaxFF potential as implemented within the LAMMPS code.[40] We carried out simulations mainly in two areas: oxidation process and mechanical tensile loading. The simulated system is similar to that we previously used to study the mechanical deformation mechanism of oxidized-Fe NWs as a function of surface oxide shell layer thickness under tensile loading.[17] The Fe lattice has a BCC crystalline structure, with a lattice constant a = 2.86 Å. To perform the simulation, an initial size of orthogonal periodic MD simulation box has been chosen $(50 \times 50 \times 50) \times a$, using this lattice constant a = 2.86 Å, that results in a size of 14.315 nm in each direction in the Cartesian coordinate system. The initial configurations of the cylindrical metallic Fe NW with a diameter of ~5.0 nm and a length of ~14.3 nm are schematically shown in Fig. 1, where red color represents Fe atoms. The diameter-to-length aspect ratios of the pure Fe NW is ~1 : 3, and contains a total of 24 050 iron atoms. The metallic Fe NW is placed in the middle of an MD box in [001] oriented direction. First, a comparative investigation of oxidation process in the H_2O or H_2O_2 molecular environments is conducted under same conditions. H_2O and H_2O_2 molecules are separately used as the two different oxidizing environments to oxidize the metallic Fe NWs. Before starting oxidation simulations, 1334 H_2O molecules are placed in random orientations into the vacuum space at about 6 Å far from the Fe NW surface, as shown in Fig. 1. Then, we allowed oxidation to occur to form a pre-oxide shell layer. All oxidation process simulations were carried out at a temperature of 300 K using a canonical ensemble (*NVT*) with a Nose–Hoover thermostat.[41] The simulation of the oxidation of the metallic pure Fe NW was

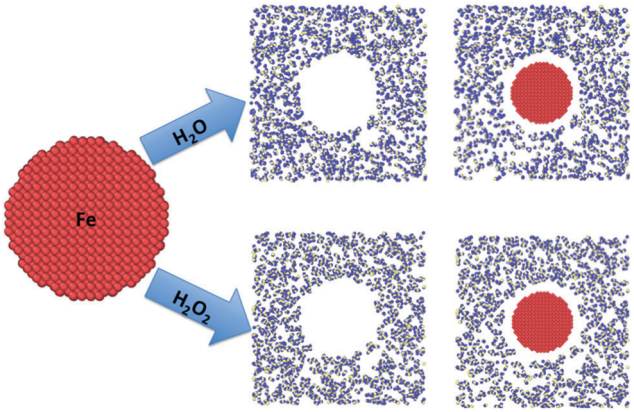

Fig. 1 Schematic diagram illustrating the initial pristine Fe NWs in contact with molecular H_2O_2 or H_2O environments. The red, blue and yellow atoms are Fe, H and O, respectively.

performed with periodic boundary conditions in all directions. Consequently, thin oxide shell layers are formed on the free surfaces of pure Fe NWs during the oxidation simulations. The H_2O molecules which did not contribute to the formation of the oxide shell layer were then removed from the simulation box. The same set of oxidation simulations with the same conditions were then repeated in the H_2O_2 molecular environment, initially containing 1000 H_2O_2 molecules in the vacuum region. The oxidation simulations with the H_2O and H_2O_2 oxidizers were run for 0.4 and 1.1 ns, respectively. Over the duration of simulations, total number of 3764 (2509 H and 1255 O atoms) H_2O and 3736 (1866 H and 1870 O atoms) H_2O_2 molecules were consumed to form the oxidation shell layers. The resulting oxide shell layer with different phases ($Fe_xO_yH_z$) is formed on the free surfaces, depending on the oxidizer. The snapshots of Fe NW before (Fig. 1) and after oxidation (Fig. 2) are presented to illustrate the atomic configuration of the oxidation process as well as the resulting oxide shell layers on the free surface of NWs.

Once the pure and pre-oxidized Fe NWs were reacted with H_2O or H_2O_2 (two different surface oxide phases), the tensile mechanical deformation simulations were performed in two steps similar to our previous work.[17] Prior to performing the tensile test, starting from the initial configuration, first, energy minimization is performed for all NWs using the conjugate gradient method to obtain the minimum energy configurations. Next, we carried out equilibration simulations with a Nose–Hoover isobaric–isothermal (*NPT*) thermostat at T = 300 K and zero pressure in the z-direction to allow structural relaxation, in order to remove surface tension due to the internal residual stresses.[42]

After the equilibration process, all Fe NWs were subjected to uniaxial tension loading along the [001] direction by applying a constant uniform strain rate of 0.01% ps^{-1} (10^8 s^{-1}). A periodic boundary condition was only applied in the loading direction in order to remove surface effects, thus resembling an infinitely long NW. In deformation simulations, all atoms were uniformly displaced in a stepwise manner until 15% of the initial box length. These simulations are performed with the *NVT* ensemble at a

constant temperature of T = 300 K using a Nose–Hoover thermostat.[41] An explicit time-reversible velocity-Verlet integrator with a time step of 0.25 fs was used to numerically integrate the equation of motions.[43] The total duration of the mechanical deformation simulations is 1.5 ns. Atomic charges were determined at every MD time step to minimize the electrostatic potential energy.[39,44]

3. Results and discussion

3.1 Resulting oxide growth processes and hydroxyl formation upon H_2O or H_2O_2 oxidation

In this work, we focus on comparison of the oxidation process of metallic Fe NW with two different oxidizing agents—molecular H_2O and H_2O_2—by carefully controlling the temperature in the *NVT* ensemble. The oxidation processes of Fe NWs with a diameter of 5.0 nm are discussed in terms of similarities and differences for the two different oxidizer environments (H_2O and H_2O_2 atmosphere) in the gas phase. The high reactivity of H_2O and H_2O_2 molecules causes rapid oxidation of Fe NW with correspondingly distinct chemical reaction paths and also to create core Fe–Fe oxide shell nanostructures. The growth of oxide shell layers changes the morphology and leads to a core–shell structure, as is clearly visible in Fig. 2. The Fe NWs oxidize more rapidly in the H_2O atmosphere than in the H_2O_2 atmosphere. The metallic Fe NW with an excess of clean surface areas readily interacts with H_2O and H_2O_2, which can be attributed to the dissociative chemisorption of H_2O and H_2O_2 molecules at the free surface sites. Notably, the complicated surface geometric nature of cylindrical NW provides an inhomogeneous distribution of adsorption sites and structures, such as different crystal orientations, vacancy defects, *etc.*, which may influence the reactivity of adsorption and dissociation process of molecules, promote specific interactions, and surface reactions. The reaction mechanisms of the oxidation process and chemical reactivity of H_2O towards Fe NW in the gas phase differs significantly from that of H_2O_2. We found that H_2O and H_2O_2 molecules react with the metallic Fe NW at specific free surface sites to readily form bonds with Fe atoms *via* both molecular interaction as well as dissociatively on the free surface of NW at room temperature.

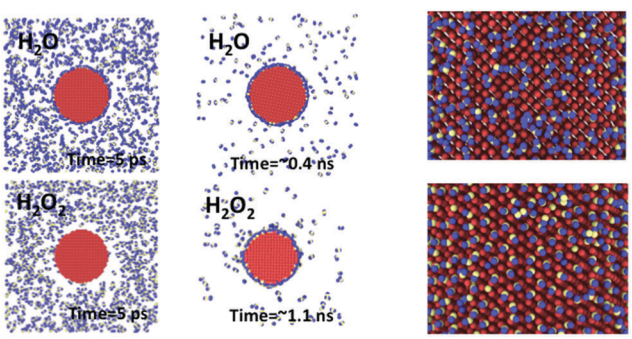

Fig. 2 The two different molecular environments used to form the core–shell ($Fe–Fe_xO_yH_z$) structure of NWs. Evolution of the formation of surface oxide shell layer depends on the nature of the molecular environments. Additionally, zoomed in snapshots of the oxide surface are also shown. The red, blue and yellow atoms are Fe, H and O, respectively.

The progressive oxidation process in the molecular H_2O atmosphere shows that the O atom of the H_2O molecule is attracted to the free surface Fe atom of the metallic NW to form weak Fe–O bonds facilitated by the difference in electron affinity between the O for Fe atoms. Therefore, most of the H_2O molecules remain in the outermost layer of the NW—without breaking O–H bonds—*via* physisorption onto the surface. Thus an ordered H_2O molecular plane is formed over the free surface of Fe NW with weak O–Fe bonding. During the continuous oxidation process, a total number of 1195 H_2O molecules are physisorbed on the free surface of Fe NWs in the form of interfacial H_2O–Fe bonds, exhibiting preferentially radially up orientation of H atoms of these H_2O molecules, leading to the polarization of the H_2O molecules. This observation can be attributed to the existence of attractive electrostatic interactions between Fe and O atoms. The vertical orientation of the H_2O molecules at the outer most surface of the NW, with O–H bonds directed towards the surface, is evident in Fig. 2. However, we also observed dissociation of a small number of H_2O molecules during the oxidation process. Approximately, a total number of 60 H_2O molecules are dissociated *via* the breaking of O–H bonds into more reactive hydroxyl (OH^-) and H ions. The result indicates that approximately only ~4.5% of the H_2O molecules are dissociated. The low percentage of hydroxyl ions relative to that of H_2O molecules also contributes to the formation of the oxide shell layer. A large difference in charge between the dissociated hydroxyl ions and Fe surface results in a stronger Coulombic interaction that helps the ions to diffuse into the core of metallic NW as well as recombination with surface Fe atoms. Thus, the hydroxyl ions can oxidize the Fe surface more easily and rapidly than H_2O molecules, and as a result, they facilitate the growth of a thicker oxide shell layer. However, the small number of dissociated ions from the H_2O molecules have relatively lesser influence on the composition of Fe oxides and the mechanical deformation mechanism. The resulting oxide shell layer primarily contains physi/chemisorped H_2O molecules and minor components of OH^- and H^+ ions. This result suggests that oxidation of the metallic Fe NW in a H_2O environment results in predominantly adsorbed H_2O molecules. As a result, there is no significant structural change in the top layer of Fe NW. We note that a total number of 1108, 60, 27 H_2O molecules are bonded primarily with one, two and three Fe atoms on the outer surface of metallic NW in the form of interfacial H_2O–*n*Fe bonds, respectively.

Our observation of the mostly physisorption of H_2O and limited degree of dissociation of H_2O molecules on the Fe-NW surface are consistent with previous studies of oxidation of Fe materials with H_2O molecules. For example, Baro *et al.* investigated the absorption of H_2O at 130 K on Fe(110) using electron energy loss spectroscopy.[45] Their observation indicated that H_2O was dissociatively absorbed at low water exposures on the surface yielding hydroxyl species. Eder *et al.* studied the interaction of H_2O molecules with Fe(100) and (110)-oriented surfaces using DFT calculations.[46] These studies provided a fundamental

understanding of the initial stages of Fe oxidation and the dissociation process of H_2O on both surfaces. For example, the closed packed Fe(110) is chemically less reactive than the more open Fe(100) surface and moreover, dissociation of H_2O molecules is a weakly activated process on both surfaces. They showed that at low coverage, H_2O dissociates spontaneously into H atoms and OH groups. Dwyer *et al.* experimentally observed that the interaction of H_2O molecules with a clean Fe(110) surface led to decomposition into a mixed ad-layer of H atoms and surface OH groups at 225 K.[47] Pan *et al.* studied oxidation of iron in a molecular H_2O environment at room temperature (298 K) and under atmospheric pressure (1 atm) by using a reactive force field.[2,3] They observed that the O–H bond dissociation in some of the H_2O molecules immediately results in the generation of new chemical species (H^+ and OH^- ions) and recombination of them with Fe atoms as time progresses. They showed that Fe atoms were bonded with a collection of primarily H_2O molecules and hydroxyl groups. For example, some H_2O molecules of the top iron layers are bonded with one, two or three Fe atoms to form a crystalline-like structure of Fe oxides in near vicinity. This behaviour is largely consistent with our observations. Moreover, the OH^- ionic termination is also reported to form three types of structures with Fe atoms, which are bonded with O atoms, HO–Fe, HO–2Fe and HO–3Fe.[2,3]

During the oxidation process for the H_2O_2 system, we observe the interaction of $\sim$934 H_2O_2 (out of the initial total number of 1000 H_2O_2) molecules on the free surface of Fe NW that consequently dissociate into hydroxyl (OH^-), water (H_2O), O^{2-}, $^{\bullet}OO^{\bullet}$ and H^+ ions. After the oxidation process, we observe an overall total number of 1 $^{\bullet}OO^{\bullet}$, 42 H_2O, 43 H, 51 H_2O_2, 88 O^{2-} and 1637 OH^- ions and molecules as a result of reactions of H_2O_2 molecules with Fe in the vicinity of the oxide region. The final dissociated products are consistent with previous MD simulations with respect to the existence of oxidation products with H_2O_2 molecules. For example, Chen *et al.* observed similar spontaneous decomposition of the unstable structure of H_2O_2 molecules and the formation a large variety of reactive species such as $H^{\bullet}$, $^{\bullet}OH$, $^{\bullet}O^{\bullet}$, $^{\bullet}OO^{\bullet}$ and $^{\bullet}OOH$ during the reaction of C atoms with the reactive H_2O_2 molecules.[48] Our result indicates that the dissociation of the O–O bond of H_2O_2 is mainly accompanied by the formation of reactive OH^- ions. Primarily, three distinct species containing H and O atoms (OH^-, H_2O and H_2O_2) are observed on the free surface of Fe NW upon the oxidation process. Especially, hydroxyl (OH^-) and O^{2-} ions are highly reactive toward Fe and penetrate deep into the core region and react with subsurface and bulk Fe atoms, leading to oxidized Fe NWs.[4,17,22] Therefore, the oxidation of Fe NWs in the H_2O_2 environment exhibits a significant morphology and structural change in the vicinity of the surface oxide region. The simultaneous growth of the oxide shell layer with reactive ions triggers the formation of an un-ordered phase in the vicinity of the oxide region. Thereby, these reactive hydroxyl OH^- and O^{2-} anions play a central role in aqueous corrosion of Fe as well as influencing the degradation of the overall mechanical properties of Fe NWs.[4,22]

Our result reveals that H_2O_2 molecules interact with the metallic Fe NW more strongly to form the oxide shell layer as compared to H_2O. Specifically, the surface modification is strongly correlated with the number of dissociated molecules into reactive ions. The number of reactive ions dictates the degree of surface reconstruction and defectiveness in the oxide region. The dissolved molecules are converted into reactive ions such as OH^- and O^{2-} ions which diffuse quickly into the subsurface of NW, reacting with Fe atoms at different adsorption sites *via* charge transfer and results in significant surface reconstruction.[4] It is noted that the majority of the oxidation products in both oxidation environments are OH^- ions. As a result, the presence of the OH^- ions has the major impact on the mechanical properties of Fe NWs. In this regard, the oxide-coated Fe NW in the H_2O environment has a relatively smaller effect on the mechanical properties of the NW. Our results reveal that the oxide shell layer properties of the metallic Fe NW surface depend on the type and reactivity of oxidizing species.

3.2 Surface reconstruction: segregation and diffusion over the free surface of metallic Fe NW

In order to determine the total average thickness of the oxide shell layer, expansion of the Fe core, the density of the oxidation, the depth of penetration of the ionic species inside the core of NW (inward diffusion) and change of diameter of all Fe NWs (outward diffusion) are analysed using the atomic radial number density distribution profiles of Fe, O, and H atoms. This analysis elucidates the dynamics of the oxidation processes as well as the modification of NW structure. The core of NWs consists of only Fe atoms, while as a result of outward (Fe) and inward (O and H) diffusions, the Fe, O and H atoms are present in the vicinity of the developed oxide region at the free surface of Fe NW, as seen in Fig. 3(a)–(c). Hence, our result reveals the consequences of the outward and inward diffused species in the resulting oxidized shell layer through charge transfer process and modification of intrinsic surface properties of the Fe NWs. The modified surfaces primarily correlate with the formation of the total growth of the oxide layer and radial volume extension of metallic Fe NW. Comparison of Fig. 3(a), the density of O and H atoms of oxide-coated NW formed in the H_2O molecular environment, after H_2O–Fe reactions, show a sharper interface than for the H_2O_2 molecular environment, due to the limited mobility of the ionic reactive species on the surface. At the same time, a reduced average radial number density of O and H atoms is observed in the range between the inner radial distance (r_{inner}) of $\sim$23.4 Å to the outer radial distance (r_{outer}) of $\sim$27.6 Å for the H_2O_2 case, while the range is in between r_{inner} of $\sim$24.2 Å and the r_{outer} of $\sim$25.1 Å for the H_2O case in the oxide free surface region. The difference of the outer and inner radii indicates that the total thickness of the oxide layer are $\sim$4.2 Å and $\sim$0.9 Å for H_2O_2 and H_2O systems, respectively. It is noted that the final average diameters of oxidized Fe NW with H_2O molecules is $\sim$5.0 nm, which is very close to the initial diameter of the pristine Fe NW. The oxidation of the Fe NW with H_2O environment indicates the absence of a large number of ions and their diffusion does not result into an obvious change in the radial diameter of the

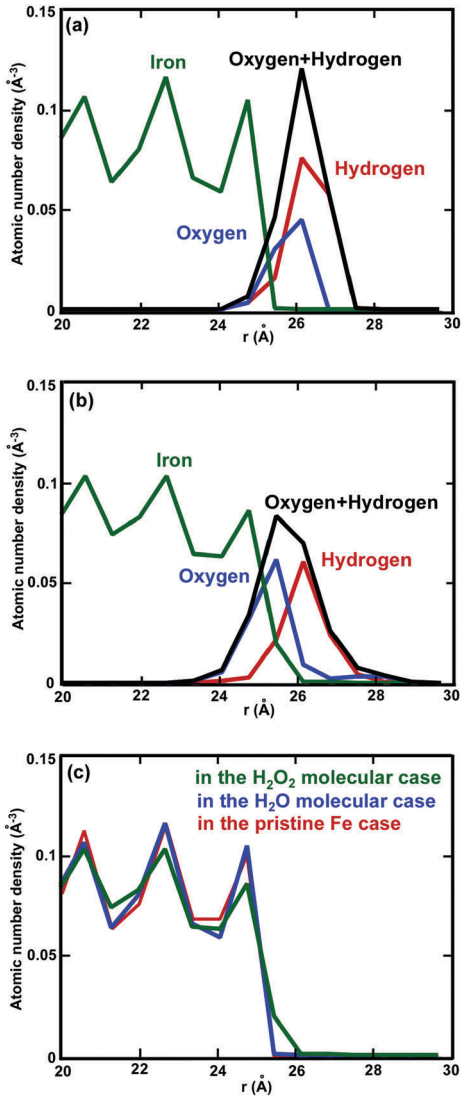

Fig. 3 The radial density profiles of Fe (solid green line), O (blue), H (red), and H + O (black) in the oxide Fe NW for (a) H_2O and (b) H_2O_2 molecules at the end of the oxidation simulation, respectively, where the radial radius *r* is the distance from the centre of NWs, with respect to each radial shell width of 0.7 Å. Further, to compare what happens on the metallic core of NW's upon the oxidation processes, (c) shows the radial density profiles of the metallic core for pure (red), oxide-coated Fe NW with H_2O (blue) and H_2O_2 (green) molecules, respectively. From these snapshots, it is seen that ionic species penetrate deeper upon the oxidation process with H_2O_2 molecules.

metallic Fe NW within our MD simulation timescales. In particular, the resulting radial number density curve of H and O atoms in the H_2O case has relatively sharp pronounced peaks and variation in their heights around the topmost free surface of the NW, which also suggest that a significant amount of H_2O molecules remain radially oriented and ordered at the free interface to form an oxide shell layer that consists solely of Fe–O bonds. Therefore, oxidized Fe NWs with H_2O molecules likely consist of a core crystalline structure of Fe NW surrounded by H_2O molecules without a significant radial extension. On the contrary, the curve shape of overall continuous radial density distributions of Fe, O, and H atoms reveals that H_2O_2 molecules exhibit stronger interactions with the metallic Fe NW. Large amounts of decomposed ionic species from H_2O_2 molecules also penetrate deeper into the core of metallic Fe NW, which causes to push the Fe atoms in a radially outward direction of the NW. As a result to accommodate this large amount of decomposed ionic species inside of the NWs, Fe atoms diffuse from the core layer to the outer surface of the NWs. It is evident that the diffusion of ionic species leads to expansion of metallic Fe NW, increase of the volume including the surface to volume ratios, large mechanical strains, and distortion of the NW in the vicinity of the oxide shell layer. Diffusion of ionic species perturbs Fe atom positions, which may facilitate the initiation of initial dislocation.[17,34] Consequently, the average radius increases from 2.5 to 2.8 nm, corresponding to an expansion of ~11%. The diffusion is associated with an increase in the molar volume, thus, the surface diffusion and the resulting thickness of the oxide shell layer formed by H_2O exposure are smaller than that for H_2O_2, in qualitative agreement with the density profiles, as clearly seen from Fig. 2. Moreover, the influence of the H_2O activity on the free surface of Fe NWs and penetration into core region is negligible compared to the H_2O_2 case.

The growth of the oxide shell layer is a synergistic process of the migration of reactive ionic species into the core of metallic Fe NW and the Fe ions toward the free surface. Thus, it is suggested that both inner and outer diffusion of ionic species in and/or out are associated with the surface chemical reactions, thus affects the size, volume, local structural, lattice distortion, density, morphologies, oxide shell layer thickness, and nanostructured roughness. As a result, each of the oxide Fe NWs in the H_2O and (b) H_2O_2 cases has a different diameter and unique crystalline Fe oxide structure. Thereby, the surface properties of oxide coated metallic NWs can be controlled by the atomic diffusion, which is driven by a strong affinity between Fe atoms to hydroxyl ions. Diffusion of ionic species associated with oxidation reactions of Fe NWs may also result in increasing of initial dislocation sites by the creation of higher defects around the vicinity of the oxide shell layer.[8,17,28] In addition to a different bonding nature of oxide atoms including phase transformation, surface stresses may play an important role in the mechanical properties of oxide-coated Fe NWs.[8] Due to the high surface-to-volume ratio of NWs, owing to the diffusion of Fe into the core region can be a reason why surface oxide has more pronounced influences on the overall mechanical strength of the oxide-coated Fe NW, resulting in a deterioration of the related mechanical properties.

The resulting unique oxide shell layer on the free surface of Fe NWs are composed of total number of 1255 O and 2509 H atoms (a ratio of ~1 : 2) for the molecular H_2O case, and 1870 O and 1866 H atoms (ratio of ~1 : 1) for the molecular H_2O_2 case, respectively. The chemical composition of the oxide-coated Fe NW is ~86.5% Fe, ~9.0% H, and ~4.5% O atoms for H_2O case in the oxide region (24.2–25.1 Å). In the molecular H_2O_2 oxidizer case, the corresponding composition is 86.6% Fe, ~6.7% H, and ~6.7% O atoms for the overall chemical composition in the oxide region (23.4–27.6 Å). Overall, a total number of 22 291 and

21 168 Fe atoms are not associated with the bonding with O and/or H atoms in the oxide surface region upon H_2O and H_2O_2 oxidizer environments, respectively. The surface oxide dependence of mechanical deformation properties is coupled with the metallic Fe core, and the Fe oxide shell layers and is explained naturally based on the overall number of oxidized/un-oxidized Fe atoms. The associated numbers (11.9% and 7.3% for H_2O_2 and H_2O, respectively) are especially significant at the nanoscale. Associated Fe atoms with oxide layer may play an interactive role between the pristine core and the oxide shell layer to explain the mechanical degradation observed in the core–shell layer of NWs. Apparently, increasing numbers are beneficial to enhancing disordered surface structures. Furthermore, we have already proved the existence of a correlation and cooperation between metallic core size and the oxide shell for oxide-coated Ni NWs.[34] At smaller diameter, the metallic Ni core experiences a greater effect from the Ni oxide shell layer, because of the higher Ni oxide-to-Ni ratio. Due to the incorporation of ionic species into the metallic Fe core, the total number of Fe–Fe bonds decreases, while the number of Fe–O/H bonds increases, which causes a reduction of metallic character in the remaining metallic core. Hence, the surface oxide structural disorder and the volume-to-surface ratio increase with the increasing diffusion depth of ionic species. We conclude that the overall number ratio of oxidized/un-oxidized Fe atoms is relatively high in the H_2O_2 oxidizer environment, which results in significant degradation of mechanical properties of the NW.

3.3 Surface phases and local structural properties of the hydroxylation shell layer associated with H_2O_2 and H_2O molecular oxidation

Herein, for a better understanding of oxide surface properties, the nature of local short-range crystalline microstructure properties and correlations of the resulting oxide shell layer on the NWs are investigated carefully by using radial pair distribution functions (RDF), coordination numbers, radial density profiles, phase composition, and morphology on the free surface of NWs.

To gain more quantitative insight into the oxide shell formation, RDFs between Fe, O and H atoms are calculated to quantify the bond lengths within the oxide regions, as shown Fig. 4 and 5. Oxidation with H_2O molecules resulted in termination of the Fe NW surface by H_2O, H^+ and OH^-. Based on the RDFs, we found the average O–H bond length including the distance between the O and H atoms in OH^- and H_2O molecules is in the range of 0.95–1.15 Å. The peak is located at 1.05 Å—slightly larger than the average O–H-bond of H_2O molecules and OH^- ions—which indicate the influence of hydrogen bonds with the surface. In addition to that, the O–H bonding suggests a slightly more ordered structuring of H_2O and OH^- within the oxide region. Relatively, a small number of the OH^- ions are segregated out from the H_2O molecules. Gutsev *et al.* calculated an O–H bond length of 0.98 Å, which is slightly longer than the experimental value of 0.96 Å.[49] The H–H partial RDF has a sharp maximal peak with large amplitude at 1.65 Å. It should be noted that the Fe–H bond length exhibits two peaks—a very weak peak at 1.7 Å, and a stronger peak appearing at 2.1 Å. The first peak is in agreement with the computational study of Liu *et al.*[50] For the dissociation of

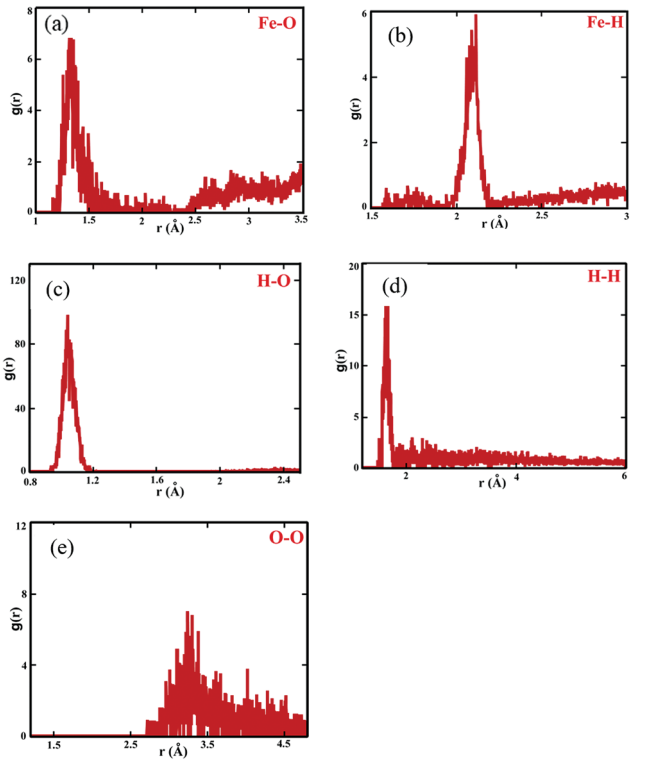

Fig. 4 RDF between (a) Fe–O, (b) Fe–H, (c) O–H, (d) H–H, and (e) O–O atoms shown for the oxide shell layer associated with H_2O molecules (21–25 Å).

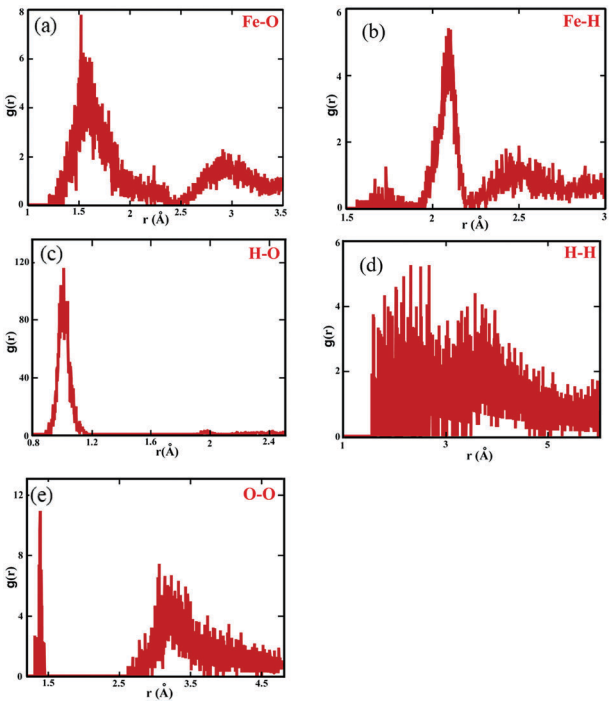

Fig. 5 RDF between (a) Fe–O, (b) Fe–H, (c) O–H, (d) H–H, and (e) O–O atoms shown for the oxide shell layer associated with H_2O_2 molecules (21–25 Å).

H atoms from H_2O molecules, they computed an H–Fe distance that is in the range of 1.63–1.68 Å, which is very close to our first peak of Fe–H. In the case of Fe–O, an intense peak occurs at 1.35 Å,

which corresponds to the presence and diffusion of OH^- ions. However, the distance between the surface Fe and O atoms vary from 1.2 to 2.5 Å, which suggests the process of hydroxylation on the free surface of Fe NW. Due to the presence of very weak chemical interactions between H_2O molecules and the metallic surface, a varying bond length in the range of ~1.8–2.5 Å is observed for the vertically-oriented H_2O molecules above the surface of NW at different facets of the cylindrical NW, indicating variations in the height of the H_2O layer above the free surface of Fe NW as well as available adsorption sites. This result is consistent with previous MD and experimental studies.[48] The experimental and simulation reported Fe–O bond lengths of hydrated ferric ions are in the range of 1.94–2.08 Å and ~1.92–2.30 Å, respectively. For example, Zhang *et al.* indicated average Fe–O bond lengths of 2.26 and 1.86 Å based on the interaction of Fe^{3+} ions with H_2O and OH^-, respectively.[51] Using density functional theory calculations and *ab initio* atomistic thermodynamics, Liu *et al.* showed that the most stable adsorption configuration of an H_2O molecule on the Fe(110) surface is at the top sites, where H_2O molecules are parallel to the Fe surface and the Fe–O distance is 2.18 Å.[52] Ossowski *et al.* reported that the H_2O molecule binds to clean and perfectly flat metallic Fe surfaces through the O atom. Our results are in agreement with their prediction of the O–Fe and O–H bond lengths that are in the range of 2.26–2.30 Å and 0.97 Å, respectively.[53] The radial distribution function in Fig. 4(e) shows that O–O bonds are not formed.

For the molecular H_2O_2 case, dissociation resulted in OH^- and H^+ ions; the OH^- species adsorbs on the Fe NW surface to form Fe–OH bonds, with dissociated H^+ leading to Fe–H bonds. The average Fe–O bond length varies in the range of 1.2–2.4 Å, but it has a distinct peak at 1.6 Å, which is slightly longer than the molecular H_2O case. In the O_2 molecular case, the Fe–O bond length was shorter as observed in a previous study on oxidation of Fe NWs with O_2 molecules.[17] For the average O–H bond length, there is a strong peak at 1.0 Å, which is closer to an average O–H-bond distance equivalent to the bond length in OH^- ions and H_2O_2 molecules. Additionally, the Fe–H bond length shows a distinct transition at 1.7 Å, which corresponds to that of the dissociated H atoms (total number of 43 H atoms) combined with Fe atoms to form the Fe–H bond, while a main average dominant peak is located at 2.1 Å. In addition to that, the average O–O bond length exhibits a sharp peak at around 1.4 Å and the second broad peak is at around 3.25 Å. The sharp peak at 1.4 Å presumably corresponds to the separation between directly bonded oxygen atoms in the existing H_2O_2 molecules at the oxide region. The H–H distribution shows absence of direct bonding.

In order to evaluate the structural changes on the metallic bonding of Fe–Fe atoms at the vicinity of the surface (21–26 Å) upon the oxidation processes, we calculate and further compare the difference between Fe–Fe overall coordination numbers and RDF before and after the oxidation process. The Fe–Fe pair correlation is split into two peaks in the initial un-oxidised case and for both oxidation scenarios, the primary peak with a bigger amplitude is located at ~2.50 Å, but with a second at relatively lower amplitude is at ~2.82 Å. The main promotional role of the formation of a native oxide surface layer leads to rearrangement of the initial crystal structure *via* the breaking and reforming of Fe–Fe bonds, which explains why there is a strength decrease for the oxide-coated Fe NWs. This is visible in that the area under the $g(r)$ of the Fe–Fe pair and the number of coordinated Fe–Fe atoms decrease for the oxide-coated Fe NWs upon the oxidation process, as is shown in Fig. 6. Surface adsorption and dissociation of H_2O_2 and H_2O molecules are the key mechanisms in perturbation of metallic Fe atoms in the vicinity of the oxide region and eventually reduced Fe–Fe coordination numbers. The positions of some atoms are considerably altered by the diffusion of ionic species and even inducing the outward diffusions of some of these Fe atoms upon the oxidation process with H_2O_2 molecules. On the contrary, most of the H_2O molecules remain mainly at the free surface of metallic Fe NW, which is not highly disturbed in the molecular H_2O environment. Thus, breaking and distortion of bonding between Fe–Fe at the vicinity of oxide region may also have a relatively insignificant role on the strength of the oxide-coated NW elastically compared to the un-oxidised counterpart. The associated number ratios are 11.9% and 7.3% for H_2O_2 and H_2O with Fe atoms, respectively, arising from the large surface-to-volume ratio. The substantial difference of the associated number ratio between H_2O_2 and H_2O molecules may probably provide a reasonable explanation why the oxide-coated Fe NW with H_2O_2 oxidizer more readily initiates partial dislocations on the free surface compared to the oxidized Fe NWs with H_2O oxidizer. This larger number indicates a significant increase in the contribution of the surface reconstruction to the overall mechanical properties of the NWs. Thus, it may play an essential role in determining their mechanical properties of oxide Fe NW deformation, especially by reducing the NW core dimensions.

Here, we also present the coordination number of Fe–H_2O and Fe–OH bonding on the resulting oxide shell layer. The integrated RDF of the Fe–O pairs up to 1.8 Å shows that the coordination of Fe atoms around O atoms of H_2O molecules is predominantly a mixture of 1-fold (total number of OFe = 1108), 2-fold (total number of OFe_2 = 60), and 3-fold (total number of OFe_3 = 27) coordinated structures, reflecting the coexistence of various phases. As a result of the continued oxidation process, the absence of diffusion suggests that most of the H_2O molecules are directly absorbed on top of the free surface of Fe NWs in the form of H_2O–Fe bonds during the hydration stage. Thereby, coordination of 1-fold FeO is the dominant structure in the oxide

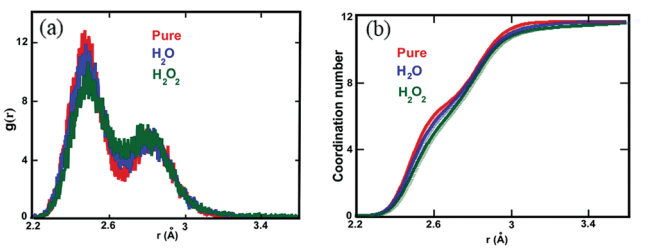

Fig. 6 Solid red, blue and green lines indicate (a) RDF between Fe–Fe atoms and (b) the coordination number of Fe–Fe atoms for pure, and oxide-coated Fe NW with H_2O and H_2O_2 molecules, respectively.

shell layer, which confirms that the coexistence of ordered H_2O molecules is attached to the one-fold sites of the outermost top site of the free surface of NW. Namely, most of H_2O molecules are directly bonded to the Fe atoms of the outermost layer. These results indicate that the chemical interactions between the H_2O molecules and the surface of Fe NW are relatively weak, that is reflected by the higher coordination number of the 1-fold structure. By contrast, the coordination of O atoms from OH^- ions with Fe atoms is 2-fold (total number of OFe_2 = 50), and 3-fold (total number of OFe_3 = 10). After the dissociation of H_2O molecules, the OH^- ions that are bonded to Fe atoms in the surface layer diffuse to the inner core of the NW. Thus, the reaction between the OH^- ions and surface Fe ions results in the formation of an oxide layer with different coordination numbers. Thus, the O atoms in OH^- ions bond with more Fe atoms, resulting in more complicated species of Fe oxides.

The composition of oxidation products in the molecular H_2O_2 case, as obtained from integrated RDF of the O–Fe pairs up to 2.4 Å indicates the coordination of O atoms around Fe atoms is predominantly a mixture of 0-fold (total number of OFe_0 = 237), 1-fold (total number of OFe_1 = 669) 2-fold (total number of OFe_2 = 752), 3-fold (total number of OFe_3 = 198), 4-fold (total number of OFe_4 = 8), and 5-fold (total number of OFe_3 = 6) coordinated structures, reflecting the loss of crystalline order, coexistence of various bonds, and formation of an amorphous layer. One-fold is the dominant crystalline phase, while 5-fold is present only in a minor quantity. Moreover, integration of the RDF of the H-Fe pairs up to 2.2 Å depicts the coordination of H atoms around Fe atoms is predominantly a mixture of 0-fold (total number of HFe_0 = 329), 1-fold (total number of HFe_1 = 1491) 2-fold (total number of HFe_2 = 19), 3-fold (total number of HFe_3 = 23), 4-fold (total number of HFe_4 = 1), and 5-fold (total number of HFe_3 = 3) coordinated structures. Due to the coordination between Fe and O and H, the oxide surface is comprised of many mixed oxide phases. This coordination number ratio changes the physical properties of the NW and makes the nanostructure more complex. Structural coordination number comparisons indicate that the formation of the oxide shell layer on the metallic Fe-NWs shows unique structural features such as the overall local oxide microstructure, types of chemical bonding, and stoichiometry, which are strongly dependent on the oxidizer environment. In comparison, the resulting oxide shell layer with the H_2O molecules do not cause a significant structural change since the most of H_2O molecules did not dissociate upon the oxidation process as compared to the H_2O_2 molecular case. In addition to that, the oxide shell layer with H_2O_2 molecules is found to retain a large number of OH groups. Comparison of the oxidation process between the molecular H_2O and H_2O_2 cases shows that the H_2O_2 molecule has a high oxidizing ability toward the metallic Fe NW, leading to more substantial modification of the free surface structure of pristine Fe NW compared to H_2O. Thus, the type of oxidizing environment influences the phase composition and microstructure of the formed surface layers. However, we find that the oxidizer species of O and H atoms are randomly distributed in the oxide region of the NWs. The cylindrical free surface of Fe NW has a surface anisotropy, which may be responsible for these random distributions. In particular, the coexistence of surface anisotropy features results in the random distributions with the oxidation process, which reflects the stochastic nature of the oxidation process.

3.4 Tensile mechanical properties of Fe NWs and oxidized Fe NWs

We have investigated the surface oxide microstructure-dependent intrinsic mechanical tensile properties of oxide-coated Fe NW with H_2O and H_2O_2 molecules. The pristine Fe NW is also considered as a reference to compare degradation of mechanical properties in the presence of the oxide shell ($Fe_xO_yH_z$) layer. We have already shown that the resulting growth of surface oxide layer on the free surface of Fe NW is structurally different for H_2O and H_2O_2 oxidizer environment. It is anticipated the local structural changes on the free surface of oxide-coated Fe NWs is likely to be correlated with the tensile mechanical properties.

The average engineering virial stresses components are used to obtain the stress–strain relations for all Fe NWs, as shown in Fig. 7.[43] The tensile mechanical deformation mechanism of all the simulated Fe NWs reveals a similar trend of the constitutive relationship in their stress–strain curves in the [001] direction. The stress–strain curve can be classified into three distinct stages: (I) a linear elastic regime, (II) a nonlinear elastic regime, and (III) a plasticity deformation regime under uniaxial tension loading. Noticeably, we observe a significant amount of structural transformation from a BCC crystal to a FCC crystal structure, which is mainly responsible for accumulation of the non-linear elastic deformation.[54,55] The twin is formed and consequently a significant number of atoms in 'FCC' configuration suddenly drops to zero. Our results for Fe NWs with and without oxide are consistent with Landau's recent uniaxial nano-deformation experimental study on pure Fe nano-pillars using high-resolution transmission electron microscopy.[16] Landau *et al.* reported qualitatively similar three stages in the tensile stress–strain curves for Fe NWs, considered as stages I, II, and III, respectively.[16] Sainath *et al.* studied the influence of temperature, ranging from 10 to 1000 K, on the tensile deformation and fracture behavior of ⟨111⟩ BCC Fe NWs using MD simulation under a constant strain rate of 1×10^8 s^{-1}.[14] Similarly, they also observed that the subsequent deformation of all the NWs exhibits non-linear deformation behaviour after the initial linear elastic regime until the onset of the plastic deformation regime at relatively high strains $> \sim 0.04$, which is in close agreement with our linear yield strain values. Notably, non-linear deformation highly depends on the temperature of the system. The microstructure of the surface oxide coating influences the stress–strain curves resulting in the different levels of strain and stress, as shown clearly in Fig. 7. The oxide coating significantly reduces the strength of NWs as is evident from the reduction of the linear and maximum critical yield stress and strain. The extracted mechanical properties of all Fe NWs are shown in Table 1. Importantly, the similarity of stress responses for all NWs implies that tensile mechanical deformations in all cases have the same tendency, involving a similar deformation mechanism.

In the linear elastic region for all NWs, the stress increases linearly with the increase of strain until it reaches the linear

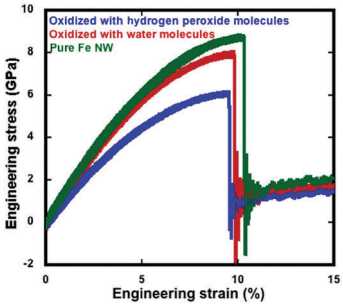

Fig. 7 Engineering stress–strain curve for pure (solid green line), oxidized Fe NWs with H_2O (solid red line) and H_2O_2 (solid blue line) molecules, respectively. It can be seen that the NWs oxidized in two types of oxidizer environment exhibit different effects on the mechanical degradation of core–shell structures.

yield state. In regime II, in between the linear yield strain and maximum critical strain level, this corresponds to the nonlinear elastic region where the stress varies slowly in a nonlinear manner with the increasing strain. As soon as the strain reaches the maximum critical yield strain level, twin seed (defects) start to nucleate from the free surface and/or interface region, resulting in the onset of plastic deformation. Near the maximum critical yield state; further increases in the strain cause a sharp drop of stress to a relatively lower value. Beyond the maximum critical yield state the NWs deform plastically in a ductile manner in regime III with increasing strain. In addition to this, the variation of flow stress level remains relatively constant at low-stress level and fluctuates around the average value due to twinning deformation. The flow stress value of the pure Fe NWs is consistent with the results of Li *et al.* and Landau *et al.*[16,55]

Table 1 presents the tensile mechanical properties of all the Fe NWs. The corresponding linear yield strains and stress values are 6.0, 4.9 and 4.8% and 6.8, 5.6 and 4.3 GPa for the pristine, oxide-coated Fe NW with H_2O, and oxide-coated Fe NW with H_2O_2, respectively. The pristine Fe NW exhibits significantly higher linear yield strain and yield stress relative to their oxide counterparts. The drop of linear yield stresses is shifted to lower strain value as compared to the pristine Fe NW. Especially, oxide NW with H_2O_2 molecules requires less work to overcome the linear yield stress barriers in comparison to the H_2O case. This observation could be due to the relatively increased potential defects on the free surface of Fe NW in the H_2O_2 system, as compared to that of the pure and H_2O coated Fe NWs. Moreover, the corresponding maximum critical strains are about 10.4, 9.8 and 9.6% and maximum critical stresses are 8.7, 8.0 and 6.0 GPa for the pristine, oxide-coated Fe NW with H_2O and H_2O_2, respectively. In the absence of any surface oxide layer, the Fe NW is mechanically hard. The onset of plastic deformation for oxide-coated NW with H_2O_2 molecules is slightly shifted to lower maximum critical strain levels. The required maximum critical stress to commence plastic deformation decreases from 8.7 GPa to 6.0 GPa ($\sim$31%) for the oxide shell layer formed by H_2O_2 as compared to its pristine counterpart while the corresponding change is less significant ($\sim$8%) for H_2O. The results indicate that the oxide local microstructure types on the free surface of crystalline metallic cylindrical Fe NWs are strongly correlated with the initiation of initial dislocation. The initiation of dislocations results in a reduction on the onset of the plastic deformation as well as the tensile intrinsic mechanical properties of Fe NWs including the linear yield strain and the stress, and the maximum critical yield strain and stress. Thus, the oxide-coated NW with H_2O_2 molecules shows significantly lower maximum critical stress at the final inelastic deformation stage. Oxide-coated with H_2O_2 molecules thereby make the NW easier to deform in the elastic regime, and consequently leading to a lower elastic modulus. Once plastic deformation is begun for all NWs, the nucleation and growth of twinning occurs at a relatively smaller stress value, but it fluctuates almost at a constant value of the flow stress, as seen from the stress–strain curves.[14,17,55] The work of hardening rate of all the Fe NWs is obtained by integration of the area under the tensile stress-strain curves.[33] The oxide shell layer including local structure has an effect on the work of hardening rate as is observed from the tensile stress–strain curves. Our result is consistent with the previous MD simulation studies of plasticity for Fe NWs, for example, a large maximum stress is required to onset the plastic deformation, which creates the twins initially, but subsequently follows the tensile twinning process with comparatively lower stress as strain increases.[17,55]

The Young's modulus values are found to be 114.8, 117.0 and 91.9 GPa for the pristine, oxide-coated with H_2O and H_2O_2 molecules, respectively. The comparison of the Young's modulus indicates that the onset of softening depends on the surface microstructure. For example, the absorption of H_2O molecules on the free surface of metallic Fe NW is relatively weak. Therefore, it is covered by mostly H_2O molecules, which only slightly affect the Young's modulus. Most importantly, the Young modulus of oxide-coated Fe NW with H_2O_2 molecules is considerably lower than its pristine counterpart, namely $\sim$20%. Plastic deformation of the oxide-coated Fe NW with H_2O_2 molecules starts at a lower stress value as compared to the pure Fe NW and oxide-coated with H_2O molecules. This implies significant structural changes in the vicinity of the free surface of Fe NW during the oxidation process with H_2O_2 molecules. Thus, the softening effects and mechanical strength in Fe NWs are correlated with the resulting oxidation shell layer microstructure. On the other hand, there is a relatively small difference in the Young's modulus between the pure Fe NW and oxide with H_2O molecules.

Table 1 Mechanical properties of the pure and oxide-coated Fe NWs with H_2O and H_2O_2 molecules at constant strain rate. The values of linear yield strain (ε_z^{lin}), linear yield stress (σ_z^{lin}), maximum critical yield stain (ε_z^{max}), maximum critical yield stress (σ_z^{max}), and Young's modules (E) are shown. Two different oxidizing environments are used to the formation of the oxide shell layers

System	ε_z^{lin} (%)	σ_z^{lin} (GPa)	ε_z^{max} (%)	σ_z^{max} (GPa)	E (GPa)
Pure	6.0	6.8	10.4	8.7	114.8
H_2O molecules	4.9	5.6	9.8	8.0	117.0
H_2O_2 molecules	4.8	4.3	9.6	6.0	91.9

In addition, chemical reactions during the oxidation process causes the crystalline symmetry to be broken on the free surface, with exchange of bonds of surface atoms, the reduction of coordination number, changes of chemical variations, stoichiometry and local structure of the oxide shell. Diffusion of atoms into the oxide region may account for at least some of correlated defects at the interface and/or oxide region, which acts as a productive source to initiate initial dislocation sites as well as act as a corrosion initiation sites, thus promoting the initial activities of partial dislocations.[17,23,34] Namely, the diffusion of ionic species breaks the symmetry and opens up a number of possible dissociation sites within the vicinity of the oxide shell layer that could act as an activator for the initiation of initial dislocations to onset plastic deformations. Thus, the aforementioned issues lead notably to the different mechanical deformation properties distinct from those for pristine counterparts. Thereby, mechanical strength and properties of the metallic Fe NWs can be controlled effectively by simply controlling the oxide surface layer local microstructure associated with the oxidizer environment.

There are several studies that indicate the existence of H_2O and H_2O_2 molecules degrades the mechanical properties of nanomaterials.[20,56,57] For example, Khoei *et al.* studied the mechanical properties of pristine graphene and graphene oxides at various percentages of O, OH and O/OH under tensile and shear loadings using MD simulations.[56] They indicated that the increase of the oxide agents facilitates the reduction of the Young modulus and the ultimate tensile stress in the graphene sheet, and the failure behavior of the graphene sheet changes from brittle to ductile. Verners *et al.* studied stress corrosion properties and the dislocation behavior of Ni nano plates structures in H_2O environment using the ReaxFF potential.[57] In similarity with our observations, they indicated that the reaction of H_2O molecules with metallic Ni results in the reduction of dislocation nucleation barriers, *e.g.* the tensile stress barriers, as well as reduction of overall material strength and ductility, as compared to pristine Ni plates in a vacuum.

3.5 The role of oxidation on tensile deformation behaviours of metallic Fe NWs

To obtain a comprehensive insight into the existence and movement of dislocation activities occurring inside the deforming NWs, the evolution of defect structures of the NW is closely monitored. In order to identify accurately the possible intrinsic plastic deformation mechanisms and further to make a comparisons, we performed the common neighbor analysis (CNA) using OVITO.[58] All the atoms are colored according to their CNA where blue, green and orange colors correspond to perfect BCC, FCC and unknown atoms, respectively. Defects associated with the local crystalline disordered atoms are in the same color at oxide region, interior defects such as dislocation core and twin boundaries. The oxidation of Fe NWs associated with H_2O and H_2O_2 molecules leads to a relatively drastic modification of the existing surface local microstructure, the homogeneity, the symmetry, and the nature of the unique chemical bonding at the oxide of free surface and/or interface in between the oxide and core region. Furthermore, the free surface of Fe NWs is covered by heterogeneous crystalline oxide structures, which depends on the type of oxidizer environment. In this regard, the resulting oxidation processes lead to an increase of the number of initial dislocation emission sites on the oxide shell layer as well as at the interface between the core and shell. The aid of more active dislocation emission sites reduces effectively the activation barriers for the initial emission of partial dislocations to trigger the plastic deformation process. Overall, these active sites are potentially more sensitive to activate the initial dislocation sources at stress values below the maximum critical stress to initiate the plastic deformation mechanism. Therefore, the presence of the oxide layer acts initially as sources and sinks to facilitate, as well as accelerate, the onset of plastic deformation mechanisms by assisting initiation of initial dislocation activity, *i.e.*, the reduction of maximum critical stress. Specifically, activation of initial dislocations strongly depends on the stress state of the free surface and interface, which is modified upon the oxidation process using different reactive oxidizers. Thus, the largest stress concentrations mainly shift to these oxide imperfection sites, and thereby, initiation of defects will preferentially start at the energetically favorable edges on the free surface, oxide region, and/or interface regions of the NW where the local maximum stresses exist. Especially, the presence of the oxide layer decreases corresponding yielding stress in complex ways, to begin the initial dislocation activities based on mechano-chemical reactions, thereby, softening the oxide Fe NWs.[17,33,34] Comparison of our results, shows in particular, the resulting oxidation of Fe NW with H_2O_2 molecules provides relatively very little mechanical resistance to the onset of the plastic deformation, which occurs at a low-stress level due to the significant surface modifications. It indicates that the number of initial dislocation sites is relatively higher in case of the oxidation with H_2O_2 than that with H_2O to nucleate initial dislocations.

The onset of plasticity for the [001] oriented pure and oxide Fe NWs is promoted specifically by nucleation through partial dislocation on the {112} crystallographic glide planes.[14,17,31,55,59] However, the yielding to the onset of plastic deformation for the oxidized Fe NWs occurs at relatively lower strain and stress values than that of the pure NW, *i.e.*, the mechanical resistance to plastic deformation decreases. Initial dislocations emission considered as nucleation of twin seeds commences from the free surface, oxide shell layer and/or interface to onset plastic deformation. Then, the nucleation and the growth of parallel partial dislocations occurs on $\langle 111 \rangle$ {112}-glide planes bounded by dislocation loops. Once a dislocation is initiated, increasing the applied tensile strain, consecutive and continuous motion of closed partial dislocation loops commences to propagate laterally from one surface toward the opposite ends of the free surface of the NW along the restricted glide plane. Finally, they encounter at the opposite surface of the NWs to form a pair of stacking faults to realize a twin. Subsequently, with further increasing the strain, this results in the formation of a pair of parallel high symmetry stacking faults considered as twin boundaries (coherent twin interfaces), as is seen in Fig. 8 and 9. It is noteworthy that the nucleation of closed dislocation

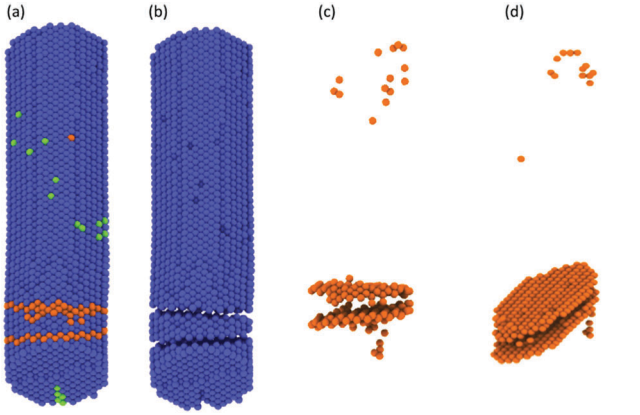

Fig. 8 The successive nucleation, growth, propagation and thickening of twinning in the oxide NW with H_2O_2 molecules based on CNA under mechanical tensile loading. The green, blue and orange colours represent FCC, BCC, and the unknown (amorphous) structure atoms, respectively. (a) The surface unknown structure atoms are removed from the full NW to show the interior perfect BCC atoms and the defects. The perspective view shows the initiation and evolution of the deformation at the interface; and (b) only BCC atoms are shown. For clarity, (c and d) only the interior defective atoms (unknown atoms) in the NW are shown from different perspectives.

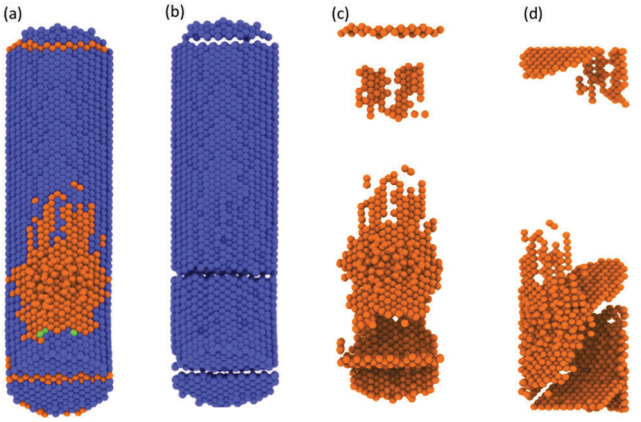

Fig. 9 The successive growth, propagation and thickening of twinning, as the strain increases further in the oxide NW with H_2O_2.

loops and formation of the twin on the coherent twin boundary are observed for all Fe NWs. Surprisingly, the abrupt crystallographic lattice reorientation in between the closed dislocation loop begins immediately with the formation of the initial closed dislocation loop. Namely, the nucleation of a dislocation loop and subsequently formation of twinning converts the elastic to plastic deformation process. At the same time, the ductile behaviour and softening of plastic deformation of all Fe NWs are achieved vertically and laterally through the repeated nucleation, formation, growth, propagation and thickening of twinning, which are restricted in between its existing internal twin boundaries. The imposed constant strain rate is entirely maintained by only one pair of twinning boundaries including the gliding partial dislocation defects on the twin boundaries during tensile mechanical loading. The similarity of subsequent propensity for dislocations glides on the primary slip system {112} atomic planes was commonly observed. In particularly, only a pair of twin boundaries is activated within the wires, the $(1\bar{1}\bar{2})$, (112) and $(1\bar{1}2)$ slip planes for oxide-Fe NWs with H_2O and H_2O_2 molecules and pristine NW, respectively.

We also observe some minor dislocation activities. The strain evolution of the plastic deformation mechanisms in the oxide-NW with H_2O_2 molecules is presented in Fig. 8 and 9, which gives a detailed picture of the inhomogeneous nucleation of dislocations as the initiation of twin seeds from the oxide region, formation of stacking faults, and thickening processes of the twin slab. In the case of H_2O_2 oxidized NWs, nucleation of two twin seeds is created initially from the oxide shell layer of the NW to onset the plastic deformation, as is seen in the snapshot of Fig. 8. As the deformation continues, one of the twin seed was lived for a short period and then disappeared in the NW. It is worth noting that another twin seed is rapidly able to complete the formation of a twin in the NWs (Fig. 8(c) and (d)). Finally, the twin boundaries with a width of two atomic layers are formed along the longitudinal axis for all NWs, which are divided in all the NWs into two domains by forming a (112) twin plane one in between twin boundaries with new lattice orientations, as shown in Fig. 8 and 9.

Relatively large maximum critical stress associated with the assistance of external forces is required for the formation of a twin.[14,55] Subsequently, the majority of further evolution of plastic deformation continues *via* twinning progression, which occurs readily by relatively small constant twin-propagation stress values, implying that the high propensity of the propagation of twin boundaries is consistent with previous observations.[14,31,55,59] On the other hand, onset of plastic deformation processes associated with the distortion of the stress–strain curve (sharp decline in the stress–strain curve) results in relieving high stress of the NW, which coincides with the generation and the subsequent propagation of partial dislocations. Additionally, the lattice reorientations within the existing twin boundaries (the twinned domains) occur progressively into a new orientation of [011] axis with respect to the initial orientation of [001] axis in each NW. The actual lattice orientation and re-orientation in between twin boundaries are seen in Fig. 8 with the increase of tensile strain during the twin propagation. Lattice reorientation through twinning on the twinned domain planes proceeds during the plastic deformation process. However, local configuration remains in BCC structure inside the NW, and no structural phase transition occurs for all Fe NWs during the entire plastic deformation process except at the twin boundaries and oxide region. Thus, an atomic reorientation in between the existing closed dislocation loop and consequently the existing twin boundaries associated with flow stress moves collectively in the same direction to accommodate the plastic strains during the rest of the tensile loading. Consequently, the simultaneous occurrence of twin migration and the changes of twinned grain reorientation are responsible for the ductile and softening plasticity of all Fe NWs, implying that twinning process is the dominant mechanism to facilitate the plastic deformation process. The increasing and/or decreasing length of twin boundary spacing including lattice re-orientations in consequence, which are also associated with crystallographic reorientations of the free

surfaces of NWs, results in relatively small continuous zigzag-shaped structures behavior around a mean stress value.[55] Likewise, NW can adjust the overall twinning stress relatively easily by changing its free surface orientation and increasing the surface areas as well as re-orientation of twin domains, which is collaborated by the propagation of dislocation. Only one twin is created, which is responsible for the overall plastic deformation.[55]

The substantial differences in the linear yield and maximum critical stresses values indicate that the maximum yield stresses are correlated with surface local oxide microstructures, which are significantly different from each other. Namely, the surface oxide layer promotes initiation of deformation twinning but not the overall subsequent plastic deformation behavior. On the other hand, the plastic deformation mechanism of all NWs is dominated by deformation twin progression, which is not changed significantly by the existence of the oxide layer. Thereby, the plastic deformation behaviors and evolution trends are qualitatively quite similar to absorb external stress regardless of the presence or absence of surface oxide during the plastic deformation process. Moreover, with the onset of plastic deformation, maximum stress associated with a high resolved shear stress acted as the driving force to provide high mobility as well as glide quickly the partial dislocation and the twin boundaries. Therefore, beyond the initial dislocation emission, the oxide local microstructure has the ability to control the initial cross-slip partial dislocations propagation speeds to form the twinning. Thus, twinning activities facilitate as well as control the overall plastic deformation and the mechanical ductability of all the Fe NWs.

To the best of our knowledge, there are no experimental and simulation results published on the effects of the pre-oxide Fe NW with H_2O and H_2O_2 molecules on the tensile deformation mechanism and related properties. Therefore, we make some qualitative comparisons, which very well confirm the overall trend in mechanical deformation process for only pristine [001] oriented Fe NWs. We remark that our results for the overall plastic deformation mechanism and behaviour also exhibit quantitative similarities as well as agreements with the previous simulations and experimental studies.[14,17,31,55,59] These studies suggested that the mechanical deformation mechanism and related properties in BCC Fe NWs and nanopillars are quite sensitive to orientation, applied strain, temperature, and pre-existed defects. These observations indicate that the ductility and softening of plastic deformation process are associated with complex twinning-dominated mechano-chemical reactions, which undergo stochastic collective behaviours including the initiation and motion of partial dislocation, followed by formation of a pair of twin boundaries.[17] It is also noteworthy that surface defects contribute to activating initial dislocations more easily. Generally, previous simulations revealed that single crystal BCC Fe NWs experience primarily similar deformation processes, which also indicated that the twinning on the slip system {112} atomic planes is the dominating plastic deformation mechanism at high strain rates and low temperatures during tensile loading.[17,55] Following yielding, twin thickening at the coherent boundaries requires other mechanisms such as the decreasing/increasing twin boundary pair spacing assisted by atomic specific re-orientations, changing geometrical and crystallographic reorientation of NW surface, and increase of the free surface area of NW in the plastically deformed region.

4. Summary and concluding remarks

In conclusion, employing MD simulations with ReaxFF potential, we demonstrate comparatively the importance of the resulting surface oxide shell layer on the mechanical properties of metallic Fe NW. First, we investigated the oxidation process of the metallic Fe NW in the presence of two oxidizer environments (H_2O and H_2O_2 molecules). Our results show that the local unique microstructure and morphology of pre-oxide shell layer are highly contingent on the types of oxidizing species in question, obtaining different oxide phases. Especially, the dissociation and chemisorption of H_2O_2 on Fe NW modifies the NW surface, and thus exhibits significantly different mechanical properties compared to the pristine Fe NW. The mostly physisorption of H_2O on the Fe-NW surfaces—consistent with previous studies—has a relatively lesser effect on the mechanical characteristics compared to the H_2O_2 case.[2,3] Our study reveals an interesting correlative dependence between the surface oxide local microstructure and mechanical deformation properties under uniaxial tensile loading. It is noteworthy that the surface oxide layer spawns increased the amount of initial dislocation nucleation and emission sources to dictate the plastic deformation of NW compared to the pristine Fe NW. Particularly, the amount of yield stress is reduced significantly to initiate the plastic mechanical deformation process, which fundamentally correlates with the degradation of mechanical strength and related properties of the cylindrical Fe NWs. Thus, oxide-coated Fe NWs exhibit interesting and distinctly different mechanical properties from the un-oxidized counterpart. Our results indicate that the surface oxide shell layer microstructure controls fundamentally the initiation of initial dislocations to onset plastic deformation, which in turn largely governs and manipulates the strength of the metallic Fe NW. This microstructure will depend on the type of oxidizer environments such as H_2O_2 or H_2O, used in the direct oxidation process. Our study provides an understanding of oxidation and its effects on the mechanical properties as well as the evolution of the resulting mechanical response of Fe NWs on the atomic scale. Understanding of such atomistic knowledge may have significant practical implications associated with the corrosion and oxidation processes, mechanical reliability, predictability and tolerance of Fe/Fe-oxide-related devices in inhospitable aqueous environments, and in nano-applications.

Conflicts of interest

There are no conflicts to declare.

Acknowledgements

This work was supported by The Scientific and Technological Research Council of Turkey (TUBITAK)-BİDEB 2219 under the

1059B191400364 grant. Simulations were carried out using the facilities at TUBITAK ULAKBIM, High Performance and Grid Computing Center (TR-Grid e-Infrastructure) and ITU National Center for High Performance Computing (UHEM). S. O. acknowledges the support by the Elements Strategy Initiative for Structural Materials (ESISM) and JSPS KAKENHI Grant Nos. JP17H01238 and JP17K18827.

Notes and references

1 Z. Ai, Z. Gao, L. Zhang, W. He and J. J. Yin, *Environ. Sci. Technol.*, 2013, **47**, 5344–5352.
2 T. Pan and A. C. T. van Duin, *Mater. Lett.*, 2011, **65**, 3223–3226.
3 T. Pan, *Chem. Phys. Lett.*, 2011, **511**, 315–321.
4 W. Xiang, B. Zhang, T. Zhou, X. Wu and J. Mao, *Sci. Rep.*, 2016, **6**, 24094.
5 Y. P. Ivanov, A. Alfadhel, M. Alnassar, J. E. Perez, M. Vazquez, A. Chuvilin and J. Kosel, *Sci. Rep.*, 2016, **6**, 24189.
6 M. Aryanpour, A. C. T. van Duin and J. D. Kubicki, *J. Phys. Chem. A*, 2010, **114**(21), 6298–6307.
7 A. Ali, H. Zafar, M. Zia, I. U. Haq, A. R. Phull, J. S. Ali and A. Hussain, *Nanotechnol., Sci. Appl.*, 2016, **9**, 49–67.
8 M. Kaur, J. S. McCloy, W. Jiang, Q. Yao and Y. Qiang, *J. Phys. Chem. C*, 2012, **116**, 12875–12885.
9 W. Wu, Q. He and C. Jiang, *Nanoscale Res. Lett.*, 2008, **3**, 397–415.
10 K. H. Chew, R. Kuwaharac and K. Ohno, *Phys. Chem. Chem. Phys.*, 2018, **20**, 1653.
11 K. Gandha, J. Mohapatra, M. K. Hossain, K. Elkins, N. Poudyal, K. Rajeshwar and J. P. Liu, *RSC Adv.*, 2016, **6**, 90537–90546.
12 J. Yue, X. Jiang and A. Yu, *J. Phys. Chem. C*, 2012, **116**, 8145–8153.
13 Y. Jia, T. Luo, X. Y. Yu, B. Sun, J. H. Liua and X. J. Huang, *RSC Adv.*, 2013, **3**, 15805–15811.
14 G. Sainath and B. K. Choudhary, *J. Appl. Phys.*, 2017, **122**, 095101.
15 P. Chowdhury and H. Sehitoglu, *J. Eng. Mater. Technol.*, 2018, **140**(2), 020801.
16 P. Landau, Q. Guo, P. Hosemann, Y. Wang and J. R. Greer, *Mater. Sci. Eng., A*, 2014, **612**, 316–325.
17 G. Aral, Y. J. Wang, S. Ogata and A. C. T. van Duin, *J. Appl. Phys.*, 2016, **120**, 135104.
18 K. Rout, M. Mohapatra, S. Layek, A. Dash, H. C. Verma and S. Anand, *New J. Chem.*, 2014, **38**, 3492–3506.
19 W. Zhu, J. Winterstein, I. Maimon, Q. Yin, L. Yuan, A. N. Kolmogorov, R. Sharma and G. Zhou, *J. Phys. Chem. C*, 2016, **120**, 14854–14862.
20 G. Zhang, Y. Liao and I. Baker, *Mater. Sci. Eng., C*, 2010, **30**(1), 92–97.
21 C. A. F. Vaz, A. Balan, F. Nolting and A. Kleibert, *Phys. Chem. Chem. Phys.*, 2014, **16**, 26624.
22 Z. Ai, L. Lu, J. Li, L. Zhang, J. Qiu and M. Wu, *J. Phys. Chem. C*, 2007, **111**, 4087–4093.
23 M. Krajewski, K. Brzozka, W. S. Lin, H. M. Lin, M. Tokarczyk, J. Borysiuk, G. Kowalski and D. Wasik, *Phys. Chem. Chem. Phys.*, 2016, **18**, 3900–3909.
24 R. Subbaraman, S. A. Deshmukh and S. K. R. S. Sankaranarayanan, *J. Phys. Chem. C*, 2013, **117**, 5195–5207.
25 B. Jeon, Q. V. Overmeere, A. C. T. van Duin and S. Ramanathan, *Phys. Chem. Chem. Phys.*, 2013, **15**, 1821–1830.
26 B. R. S. Rogne and C. Thaulow, *Philos. Mag.*, 2015, **95**, 1814.
27 H. Wu, J. J. Yin, W. G. Wamer, M. Zeng and Y. M. Lo, *J. Food Drug Anal.*, 2014, **22**, 86–94.
28 G. Sainath and B. K. Choudhary, *Comput. Mater. Sci.*, 2016, **111**, 406–415.
29 G. Sainath, B. K. Choudhary and T. Jayakumar, *Comput. Mater. Sci.*, 2015, **104**, 76–83.
30 G. Sainath and B. K. Choudhary, *Mater. Sci. Eng., A*, 2015, **640**, 98–105.
31 C. J. Healy and G. J. Ackland, *Acta Mater.*, 2014, **70**, 105.
32 F. G. Sen, Y. Qi, A. C. T. van Duin and A. T. Alpas, *Appl. Phys. Lett.*, 2013, **102**, 051912.
33 F. G. Sen, A. T. Alpas, A. C. T. van Duin and Y. Qi, *Nat. Commun.*, 2014, **5**, 3959.
34 G. Aral, Md. M. Islam and A. C. T. van Duin, *Phys. Chem. Chem. Phys.*, 2018, **20**, 284.
35 X. Li, S. Schönecker, E. Simon, L. Bergqvist, H. Zhang, L. Szunyogh, J. Zhao, B. Johansson and L. Vitos, *Sci. Rep.*, 2015, **5**, 16654.
36 T. J. Campbell, G. Aral, S. Ogata, R. K. Kalia, A. Nakano and P. Vashishta, *Phys. Rev. B: Condens. Matter Mater. Phys.*, 2005, **71**, 205413.
37 A. Hasnaoui, O. Politano, J. M. Salazar and G. Aral, *Phys. Rev. B: Condens. Matter Mater. Phys.*, 2006, **73**, 035427.
38 T. P. Senftle, S. Hong, Md. M. Islam, S. B. Kylasa, Y. Zheng, Y. K. Shin, C. Junkermeier, R. E. Herbert, M. J. Janik, H. M. Aktulga, T. Verstraelen, A. Grama and A. C. T. van Duin, *npj Comput. Mater.*, 2016, **2**, 15011.
39 K. I. Nomuro, R. K. Kalia, A. Nakano and P. Vashishta, *Comput. Phys. Commun.*, 2008, **178**, 73–87.
40 S. Plimpton, *J. Comput. Phys.*, 1995, **1**, 117.
41 G. J. Martyna, D. J. Tobias and M. L. Klein, *J. Chem. Phys.*, 1994, **101**, 4177.
42 G. J. Martyna, M. L. Klein and M. Tuckerman, *J. Chem. Phys.*, 1992, **97**, 2635.
43 M. P. Allen and L. J. Tildesley, *Computer Simulation of Liquids*, Oxford University Press, New York, 1987.
44 W. J. Mortier, S. K. Ghosh and S. Shankar, *J. Am. Chem. Soc.*, 1986, **108**, 4315.
45 A. M. Baro and W. Erley, *J. Vac. Sci. Technol.*, 1982, **20**(3), 580–583.
46 M. Eder, K. Terakura and J. Hafner, *Phys. Rev. B: Condens. Matter*, 2001, **64**, 115426.
47 D. J. Dwyer, S. R. Kelemen and A. Kaldor, *J. Chem. Phys.*, 1982, **76**(4), 1832–1837.
48 W. Chen, H. T. Duan, M. Hua, K. L. Gu, H. F. Shang and J. Li, *J. Phys. Chem. B*, 2014, **118**, 10311–10318.
49 G. L. Gutsev, M. D. Mochena and C. W. Bauschlicher, *Chem. Phys.*, 2005, **314**, 291–298.
50 S. Liu, X. Tian, T. Wang, X. Wen, Y. W. Li, J. Wang and H. Jiao, *J. Phys. Chem. C*, 2015, **119**, 11714–11724.
51 H. Zhang, G. A. Waychunas and J. F. Banfield, *J. Phys. Chem. B*, 2015, **119**, 10630–10642.
52 S. Liu, X. Tian, T. Wang, X. Wen, Y. W. Li, J. Wang and H. Jiao, *Phys. Chem. Chem. Phys.*, 2015, **17**, 8811.

53 T. Ossowski, J. L. F. Da Silva and A. Kiejna, *Surf. Sci.*, 2018, **668**, 144–149.
54 X. Ou, J. Sietsma and M. J. Santofimia, *Modell. Simul. Mater. Sci. Eng.*, 2016, **24**, 055019.
55 S. Li, X. Ding, J. Deng, T. Lookman, J. Li, X. Ren, J. Sun and A. Saxena, *Phys. Rev. B: Condens. Matter Mater. Phys.*, 2010, **82**, 205435.
56 A. R. Khoei and M. S. Khorrami, *Fullerenes, Nanotubes, Carbon Nanostruct.*, 2016, **24**(9), 594–603.
57 O. Verners and A. C. T. van Duin, *Surf. Sci.*, 2015, **633**, 94–101.
58 A. Stukowski, *Modell. Simul. Mater. Sci. Eng.*, 2010, **18**, 015012.
59 T. U. Xu, Z. Q. Zhu, S. F. Geng and H. Y. Song, *Phys. Lett. A*, 2017, **381**, 3222–3227.